

# Angular-dependent oscillations of the magnetoresistance in $\text{Bi}_2\text{Se}_3$ due to the three-dimensional bulk Fermi surface

Kazuma Eto, Zhi Ren, A. A. Taskin, Kouji Segawa, and Yoichi Ando

*Institute of Scientific and Industrial Research, Osaka University, Ibaraki, Osaka 567-0047 Japan*

We observed pronounced angular-dependent magnetoresistance (MR) oscillations in a high-quality  $\text{Bi}_2\text{Se}_3$  single crystal with the carrier density of  $5 \times 10^{18} \text{ cm}^{-3}$ , which is a topological insulator with residual bulk carriers. We show that the observed angular-dependent oscillations can be well simulated by using the parameters obtained from the Shubnikov-de Haas oscillations, which clarifies that the oscillations are solely due to the bulk Fermi surface. By completely elucidating the bulk oscillations, this result paves the way for distinguishing the two-dimensional surface state in angular-dependent MR studies in  $\text{Bi}_2\text{Se}_3$  with much lower carrier density. Besides, the present result provides a compelling demonstration of how the Landau quantization of an anisotropic three-dimensional Fermi surface can give rise to pronounced angular-dependent MR oscillations.

PACS numbers: 71.18.+y, 73.25.+i, 72.20.-i, 72.80.Jc

## I. INTRODUCTION

The three-dimensional (3D) topological insulator is a rapidly growing field of research in the condensed matter physics.<sup>1–29</sup> Because the bulk of a topological insulator belongs to a different  $Z_2$  topological class<sup>1–3</sup> than the vacuum, on the surface of a 3D topological insulator emerges an intrinsically metallic two-dimensional (2D) state which hosts helically spin-polarized Dirac fermions.<sup>1,3</sup> Besides the profound implications of those spin-helical 2D Dirac fermions on future spintronics, the topological insulator is expected to present various exotic quantum phenomena associated with its non-trivial topology.<sup>3–8</sup>

Motivated by theoretical predictions,<sup>3,11</sup> three materials have so far been experimentally confirmed<sup>12–18</sup> to be 3D topological insulators:  $\text{Bi}_{1-x}\text{Sb}_x$ ,  $\text{Bi}_2\text{Se}_3$ , and  $\text{Bi}_2\text{Te}_3$ . The angle-resolved photoemission experiments<sup>12–18</sup> have played decisive roles in indentifying the topologically nontrivial nature of their surface states. More recently, scanning tunneling spectroscopy experiments<sup>19,20</sup> have elucidated the protection of the surface state from spin-nonconserving scattering. In addition to those surface-sensitive probes, transport experiments are obviously important for understanding the macroscopic properties of topological insulators and for exploiting the applications of their novel surface state. However, capturing a signature of the surface state of a topological insulator in its transport properties has proved difficult: The surface state has been seen by quantum oscillations only in  $\text{Bi}_{1-x}\text{Sb}_x$  at a particular Sb concentration of 9%;<sup>21</sup> the universal conductance fluctuations associated with the surface state were observed only in Ca-doped  $\text{Bi}_2\text{Se}_3$  after careful tuning of the carrier density;<sup>22</sup> the Aharonov-Bohm oscillations through the surface state were observed only in very narrow nanoribbons of  $\text{Bi}_2\text{Se}_3$ .<sup>23</sup> Most often, the transport properties are dominated by the bulk conductivity due to residual carriers.<sup>22,28</sup>

In this context, we have very recently found<sup>29</sup> that the 2D surface state of the topological insulator  $\text{Bi}_{0.91}\text{Sb}_{0.09}$

gives rise to new types of oscillatory phenomena in the angular-dependence of the magnetoresistance (MR). It was demonstrated<sup>29</sup> that the oscillations observed at lower fields provide a way to distinguish the 2D Fermi surface (FS) in  $\text{Bi}_{0.91}\text{Sb}_{0.09}$ , while another type of oscillations of unknown origin was found to become prominent at higher fields. In the present work, we have tried to elucidate whether this new tool, the angular-dependence of the MR, can distinguish the 2D surface state in  $\text{Bi}_2\text{Se}_3$ , which is believed to be the most promising topological insulator for investigating the novel topological effects because of its simple surface-state structure.<sup>11,14</sup> We observed pronounced angular-dependent oscillations of the MR in an  $n$ -type  $\text{Bi}_2\text{Se}_3$  single crystal with the carrier density  $n_e = 5 \times 10^{18} \text{ cm}^{-3}$ , but our detailed analysis clarified that the observed oscillations are solely due to the Landau quantization of the anisotropic bulk FS of this material. Nevertheless, to the best of our knowledge, such an angular-dependent MR oscillations in a 3D material has never been explicitly demonstrated in the literature, so the present results nicely supplement our general understanding of the angular-dependent MR oscillation phenomena. In addition, our analysis provides a solid ground for discriminating the contributions of the 2D and 3D FSs in the angular-dependence of the MR in future studies of  $\text{Bi}_2\text{Se}_3$  single crystals with much lower carrier density.

## II. EXPERIMENTAL DETAILS

High-quality  $\text{Bi}_2\text{Se}_3$  single crystals were grown by melting stoichiometric mixtures of 99.9999% purity Bi and 99.999% purity Se elements in sealed evacuated quartz tubes. After slow cooling from the melting point down to about  $550^\circ\text{C}$  over two days, crystals were kept at this temperature for several days and then were furnace-cooled to room temperature. The obtained crystals are easily cleaved and reveal a flat shiny surface. The X-ray diffraction measurements confirmed the rhombohe-

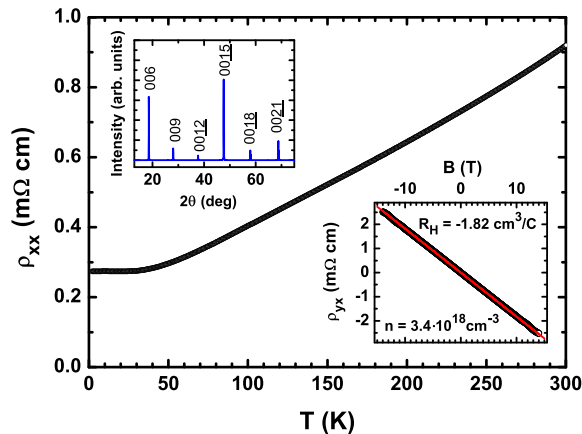


FIG. 1: (Color online) Temperature dependence of  $\rho_{xx}$  in 0 T. Upper inset shows the X-ray diffraction pattern of the  $\text{Bi}_2\text{Se}_3$  single crystal used for transport measurements. Lower inset shows  $\rho_{yx}$  for  $B \parallel C_3$  measured at 1.5 K. The slope of  $\rho_{yx}(B)$ , shown by the thin solid line, suggests that the main carriers are electrons whose density is  $3.4 \times 10^{18} \text{ cm}^{-3}$ .

dral crystal structure of  $\text{Bi}_2\text{Se}_3$ . Post-growth annealings at various temperatures under controlled selenium partial pressures were used to reduce the number of selenium vacancies that are responsible for creating electron carriers.<sup>22,28</sup>

The resistivity  $\rho_{xx}$  was measured by a standard four-probe method on rectangular samples, with the electric current  $I$  directed along the  $C_1$  axis. Continuous rotations of the sample in constant magnetic field  $B$  were used to measure the angular dependence of the transverse MR within the  $C_3$ - $C_2$  plane. For some selected magnetic-field directions, the field dependences of  $\rho_{xx}$  and the Hall resistivity  $\rho_{yx}$  were also measured by sweeping  $B$  between  $\pm 14$  T.

### III. RESULTS AND DISCUSSIONS

#### A. Resistivity and SdH Oscillations

Figure 1 shows the temperature dependence of  $\rho_{xx}$  of the  $\text{Bi}_2\text{Se}_3$  single crystal studied in this work. It shows a metallic behavior  $d\rho/dT > 0$  down to  $\sim 30$  K, and saturate at lower temperature (there is actually a weak minimum near 30 K, as is usually observed<sup>28,30</sup> in low-carrier-density  $\text{Bi}_2\text{Se}_3$ ). The single-crystal nature of the sample is evident from the X-ray diffraction data shown in the upper inset of Fig. 1. The lower inset of Fig. 1 shows the Hall resistivity  $\rho_{yx}$  measured at 1.5 K for the field direction along the  $C_3$  axis, which suggests that the main carriers are electrons and the carrier density  $n_e$  is  $3.4 \times 10^{18} \text{ cm}^{-3}$  (in a one band model). From the values of the Hall coefficient  $R_H = 1.82 \text{ cm}^3/\text{C}$  and  $\rho_{xx} = 0.28 \text{ m}\Omega\text{cm}$  at 1.5 K, the Hall mobility  $\mu_H$  is estimated to be  $6500 \text{ cm}^2/\text{Vs}$ .

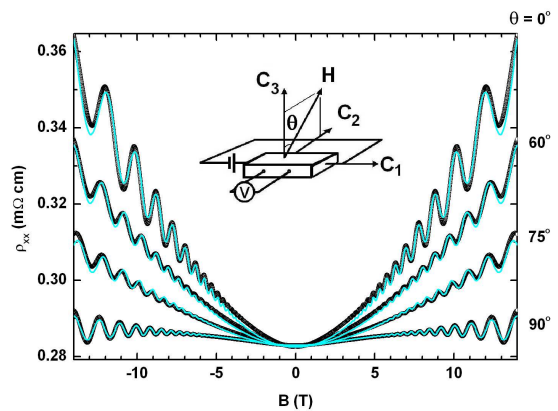


FIG. 2: (Color online) SdH oscillations measured within the  $C_3 - C_2$  plane. Thin solid lines are the result of our  $\rho_{xx}(B)$  simulation (see text). Inset shows the measurement configuration.

Figure 2 shows  $\rho_{xx}(B)$  measured at 1.5 K for several field directions in the transverse geometry ( $I \parallel C_1$  and  $B \perp I$ ), after removing the antisymmetric components due to the leakage of  $\rho_{yx}$ . Two features are evident: First, pronounced Shubnikov-de Haas (SdH) oscillations are seen for any field direction, suggesting their 3D origin. Second, the background of the SdH oscillations varies significantly with the field direction, indicating that the transverse MR is very anisotropic. Both features are taken into account in our simulation of the observed angular dependence of the MR, as will be discussed below.

Figure 3 presents the analysis of the observed SdH oscillations. The oscillations in  $d\rho_{xx}/dB$  plotted as a function of  $1/B$  for  $B \parallel C_2$  ( $\theta = 90^\circ$ ) are shown in Fig. 3(a) as an example. The very simple pattern seen in Fig. 3(a) is a result of the single frequency  $F = 107$  T (see inset for the Fourier transform) governing the SdH oscillations.<sup>31</sup> The same analysis was applied to the data for other field directions, and the obtained  $F$  as a function of  $\theta$  are shown in Fig. 3(b). The same set of frequencies can be extracted from the Landau-level “fan diagram” [inset of Fig. 3(b)], which is a plot of the positions of maxima in  $\rho_{xx}(B)$  as a function of the Landau level numbers. The slopes of the straight lines in the fan diagram give exactly the same  $F(\theta)$  as the Fourier transform result. Another piece of information that can be extracted from the fan diagram is the phase of the oscillations,  $\gamma$ , which is determined by  $\rho_{xx} \sim \cos[2\pi(F/B + \gamma)]$ . In the present case, all the straight lines in the inset of Fig. 3(b) intersect the horizontal axis at the same point, giving  $\gamma = 0.4$  that is independent of the field direction. The angular dependence of the SdH frequency  $F(\theta)$  points to a single ellipsoidal FS located at the  $\Gamma$  point with the semi-axes  $k_a = k_b = 4.5 \times 10^6 \text{ cm}^{-1}$  ( $\perp C_3$ ) and  $k_c = 7.3 \times 10^6 \text{ cm}^{-1}$  ( $\parallel C_3$ ). The expected  $F(\theta)$  for this FS is shown by the solid line in Fig. 3(b), which fits the data very well. The carrier density corresponding to this FS is  $5 \times 10^{18} \text{ cm}^{-3}$ , which is about 50% higher than that obtained from

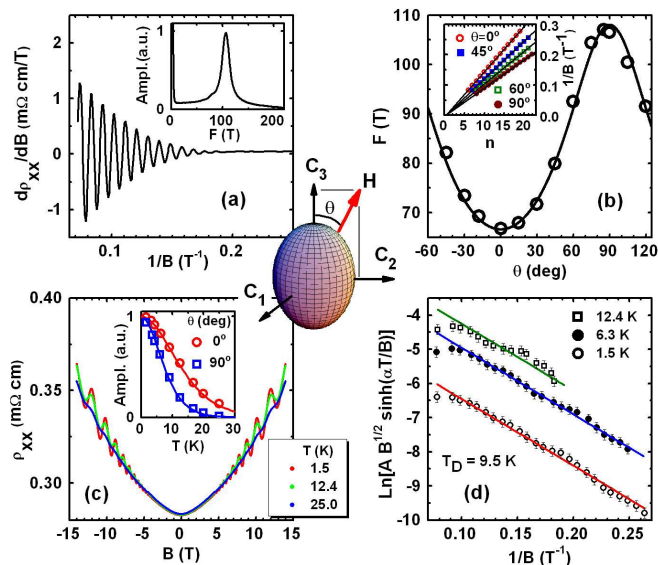


FIG. 3: (Color online) Analyses of the SdH oscillations. The inset in the middle schematically shows the obtained 3D Fermi surface and the definition of  $\theta$ . (a) SdH oscillations for  $B \parallel C_2$  as a function of  $1/B$ . The Fourier transform shown in the inset reveals a single frequency  $F = 107$  T. (b)  $F(\theta)$  measured within the  $C_3 - C_2$  plane; inset shows the fan diagram for several  $\theta$ . (c) Temperature dependence of the SdH oscillations for  $B \parallel C_3$ ; inset shows the temperature dependences of the SdH amplitudes measured along the  $C_3$  and  $C_2$  axes at 12 T, yielding the cyclotron mass of  $0.14m_e$  and  $0.24m_e$ , respectively. (d) Dingle plots for  $B \parallel C_3$  at several temperatures give the same  $T_D = 9.5$  K.

$R_H$ , as was reported previously in the literature.<sup>32</sup> This discrepancy is due, at least partly, to the fact that the present  $R_H$  was measured in the low-field limit and contains the so-called Hall factor, which is usually between 1 – 2.

The temperature dependence of the SdH oscillations was measured for two field directions, along the  $C_3$  and  $C_2$  axes. Figure 3(c) shows the  $\rho_{xx}(B)$  data in  $B \parallel C_3$  for some selected temperatures, where one can see that the background MR is essentially temperature-independent and that oscillations are still visible even at 25 K. The inset of Fig. 3 (c) shows the temperature dependence of the SdH amplitude measured at 12 T for  $B$  along  $C_3$  ( $\theta = 0^\circ$ ) and  $C_2$  ( $\theta = 90^\circ$ ). The fits with the standard Lifshitz-Kosevich theory<sup>33</sup> yield the cyclotron mass  $m_c$  of  $0.14m_e$  and  $0.24m_e$  for  $\theta = 0^\circ$  and  $90^\circ$ , respectively. The energy dispersion near the conduction band minimum of  $\text{Bi}_2\text{Se}_3$  is known to be parabolic,<sup>32</sup> and the observed anisotropy in  $m_c$  for the given FS is entirely consistent with the parabolic dispersion to within 5%. Relying on this dispersion, the Fermi energy  $E_F$  is calculated to be 56 meV and the Fermi velocity  $v_F$  is  $3.8 \times 10^7$  cm/s for any direction.

The Dingle plots [shown in Fig. 3(d) for  $B \parallel C_3$  as an example] yield the Dingle temperature  $T_D = 9.5$  K which is almost isotropic and is constant at low temperature;

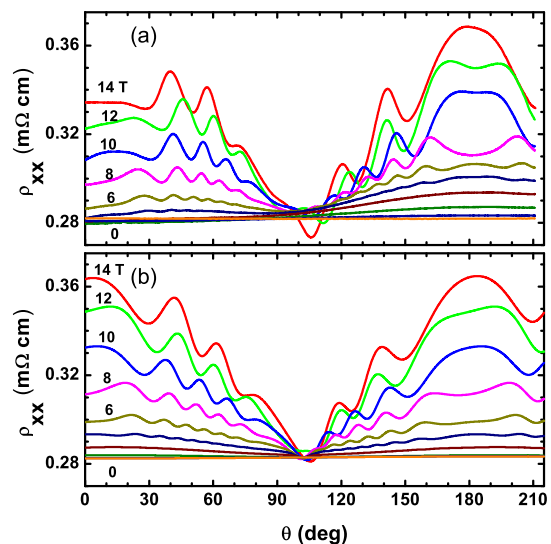


FIG. 4: (Color online) (a) Angular dependences of  $\rho_{xx}$  measured within the  $C_3 - C_2$  plane in constant magnetic fields, whose values were 0, 0.5, 1.5, 3, 4.5, 6, 8, 10, 12, and 14 T. (b) Simulation of  $\rho_{xx}$  based on Eq. (1) for the same magnetic fields as in (a).

this gives an isotropic scattering time  $\tau = 1.3 \times 10^{-13}$  s, implying the mean free path  $\ell (= v_F \tau)$  of  $\sim 50$  nm and the mobility  $\mu_{\text{SdH}}$  of about  $1600 \text{ cm}^2/\text{Vs}$ , which is almost four times smaller than  $\mu_H$  estimated from  $R_H$ . Such a discrepancy between  $\mu_{\text{SdH}}$  and  $\mu_H$  has long been noted in various systems,<sup>33</sup> and the essential reason lies in the difference in how the effective scattering time comes about from the microscopic scattering process.<sup>34</sup> The scattering rate  $1/\tau_{\text{tr}}$  determining transport properties acquires the additional factor  $1 - \cos \phi$  upon spatial averaging ( $\phi$  is the scattering angle), while  $1/\tau$  to govern the dephasing in the quantum oscillations is given by a simple spatial averaging without such a factor. Hence, if the small-angle scattering becomes dominant (which is often the case at low temperature),  $1/\tau_{\text{tr}}$  can be much smaller than  $1/\tau$ . This means that the mean free path in our sample can be even larger than that estimated above.

## B. Angular-Dependent MR Oscillations

The new observation of the present work is the oscillatory angular-dependence of the MR shown in Fig. 4(a), where, on top of the two-fold-symmetric background angular dependence, pronounced oscillations are evident at higher fields. Importantly, the peak positions shift with magnetic field, which is different from the ordinary angular-dependent MR oscillations (AMRO) in quasi-low-dimensional systems.<sup>35</sup> In the following, we show that these oscillations are due to the Landau quantization of the 3D FS and, hence, are essentially of the same origin as the SdH oscillations. The SdH oscillations occur as the Landau-quantized cylinders in the Brillouin

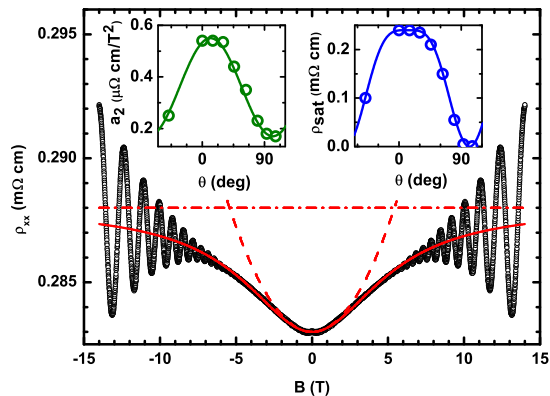


FIG. 5: (Color online) Fitting of the background MR for  $B \parallel C_2$ . Open circles show the experimental data [symmetrical component of  $\rho_{xx}(B)$ ]; the dashed line demonstrates the low-field quadratic dependence of the resistivity,  $\rho_{qd}(B) = a_2 B^2$ ; the dash-dotted line represents the high-field saturation limit,  $\rho_{sat}$ ; the solid line is the resulting reconstructed background,  $\rho_{BG}(B)$  (see text). The left and right insets show the obtained angular dependences of the coefficients  $a_2$  and  $\rho_{sat}$  within the  $C_3 - C_2$  plane.

zone expand and cross the FS with increasing magnetic field, while the angular-dependent oscillations occur as the axis of those cylinders rotates in the Brillouin zone. Obviously, no oscillation is expected for rotating magnetic field when the FS is spherical, but when the FS is anisotropic, the number of cylinders residing within the FS changes as the cylinder axis is rotated, leading to resistivity oscillations. Therefore, an anisotropy in the FS is a necessary ingredient for the angular-dependent oscillations.

To show that the observed angular-dependent oscillations are essentially due to the Landau quantization, it is most convincing to reconstruct the angular-dependence of the MR based on the SdH oscillations data. For this purpose, one needs to understand the exact magnetic-field dependence of the MR in the presence of the SdH effect, and know how it evolves when the magnetic field is rotated. Figure 5 shows the  $\rho_{xx}(B)$  data for  $B \parallel C_2$  ( $\theta = 90^\circ$ ), which we take as an example for presenting our procedure to extract the necessary information. At low magnetic fields, the MR in Fig. 5 exhibits an almost quadratic field dependence, which can be fitted by  $\rho_{qd}(B) = a_2 B^2$ . With increasing magnetic field, the MR tends to saturate, while pronounced SdH oscillations develop at the same time. The overall background MR  $\rho_{BG}(B)$  can be described as  $1/\rho_{BG} = 1/\rho_{qd} + 1/\rho_{sat}$ , which combines the low-field quadratic behavior and the high-field saturation of  $\rho_{xx}(B)$ . This background develops on top of the zero-field resistivity  $\rho_{xx}(0)$  of about 0.28 m $\Omega$ cm. The same fitting of the background of MR can be made for the whole range of the magnetic-field direction. The evolutions of the parameters  $a_2$  and  $\rho_{sat}$  with  $\theta$  in the  $C_3 - C_2$  plane are shown in the left and right insets of Fig. 5. Note that the center of the symmetry

for both  $a_2(\theta)$  and  $\rho_{sat}(\theta)$  is shifted from  $\theta = 0^\circ$  by about  $12^\circ$ , which is probably due to the rhombohedral symmetry of the crystal which leads to the appearance of cross terms<sup>36</sup> in the magnetic-field expansion of the resistivity tensor.<sup>37</sup>

Once  $\rho_{BG}$  is known as functions of both  $\theta$  and  $B$ , one can superpose the SdH oscillations to obtain the expected  $\rho_{xx}(\theta, B)$ . In the case of our  $\text{Bi}_2\text{Se}_3$ , thanks to the fact that the SdH oscillations are composed of only one frequency, one can simulate experimental data as

$$\rho_{xx}(\theta, B) = \rho_{BG}(\theta, B) \times \left( 1 + AR_T R_D R_S \cos \left[ 2\pi \left( \frac{F(\theta)}{B} + \gamma \right) \right] \right), \quad (1)$$

where  $R_T$ ,  $R_D$  and  $R_S$  are temperature, Dingle, and spin damping factors, respectively.<sup>33</sup> As shown in Fig. 2 by thin solid lines, the experimentally observed SdH oscillations are reproduced reasonably well with Eq. (1) with a parameter  $A \cdot R_S = 0.12$  which is independent of  $\theta$ .

The same set of parameters can be used to calculate the angular-dependent MR for fixed  $B$ ,  $\rho_{xx}(\theta)$ , with Eq. (1). The result is shown in Fig. 4(b), where one can easily see that the calculated angular dependences of the MR follow very closely the rather complicated patterns of the observed  $\rho_{xx}(\theta)$ . This gives compelling evidence that the angular-dependent oscillations are essentially due to the Landau quantization of the anisotropic 3D FS.

It was emphasized in Ref. 29 that a merit of measuring the angular-dependence of the MR is that at sufficiently high magnetic field, the 3D FS remains in the quantum limit (where all the electrons condense into the 1st Landau level) and do not contribute to the angular-dependent oscillations, while the 2D FS will always produce MR oscillations when the magnetic-field direction is nearly parallel to the 2D plane. Once the density of the residual carriers in a topological insulator sample is sufficiently reduced, the 3D FS should be easily brought into the quantum limit and the 2D FS would become distinguishable in the angular-dependent MR oscillations. Also, the SdH effect needs a certain range of magnetic field for the oscillations to be recognized, whereas the observation of the angular-dependent oscillations can be made only at the highest field; this gives a certain practical advantage to the latter method when the quantization condition is only barely achieved with the available magnetic field. Therefore, one would expect that the angular-dependence of the MR will be a useful tool for distinguishing the 2D surface state of the topological insulator  $\text{Bi}_2\text{Se}_3$  when a single crystal with much lower carrier density becomes available.

#### IV. CONCLUSIONS

In conclusion, we observed pronounced angular-dependent oscillations of the MR in high-quality single

crystals of  $n$ -type  $\text{Bi}_2\text{Se}_3$  with  $n_e = 5 \times 10^{18} \text{ cm}^{-3}$ . We show, by simulating the angular-dependent oscillations based on the information obtained from the SdH analysis, that the oscillations are essentially due to the Landau quantization of the 3D bulk Fermi surface. This provides a compelling demonstration of how the Landau quantization of an anisotropic 3D FS can give rise to pronounced angular-dependent MR oscillations. Furthermore, the present results pave the way for distinguishing the 2D surface state in  $\text{Bi}_2\text{Se}_3$  in future studies of the angular-

dependent MR, by completely elucidating the oscillations due to the bulk FS.

### Acknowledgments

This work was supported by JSPS (KAKENHI 19340078 and 2003004) and AFOSR (AOARD-08-4099).

- 
- <sup>1</sup> L. Fu, C. L. Kane, and E. J. Mele, Phys. Rev. Lett. **98**, 106803 (2007).
- <sup>2</sup> J. E. Moore and L. Balents, Phys. Rev. B **75**, 121306(R) (2007).
- <sup>3</sup> L. Fu and C. L. Kane, Phys. Rev. B **76**, 045302 (2007).
- <sup>4</sup> X.-L. Qi, T. L. Hughes, and S.-C. Zhang, Phys. Rev. B **78**, 195424 (2008).
- <sup>5</sup> L. Fu and C. L. Kane, Phys. Rev. Lett. **100**, 096407 (2008).
- <sup>6</sup> X.-L. Qi, R. Li, J. Zang, and S.-C. Zhang, Science **323**, 1184 (2009).
- <sup>7</sup> B. Seradjeh, J. E. Moore, and M. Franz, Phys. Rev. Lett. **103**, 066402 (2009).
- <sup>8</sup> Y. Tanaka, T. Yokoyama, and N. Nagaosa, Phys. Rev. Lett. **103**, 107002 (2009).
- <sup>9</sup> J. C. Y. Teo, L. Fu, and C. L. Kane, Phys. Rev. B **78**, 045426 (2008).
- <sup>10</sup> H.-J. Zhang, C.-X. Liu, X.-L. Qi, X.-Y. Deng, X. Dai, S.-C. Zhang, and Z. Fang, Phys. Rev. B **80**, 085307 (2009).
- <sup>11</sup> H.-J. Zhang, C.-X. Liu, X.-L. Qi, X. Dai, Z. Fang, and S.-C. Zhang, Nat. Phys. **5**, 438 (2009).
- <sup>12</sup> D. Hsieh, D. Qian, L. Wray, Y. Xia, Y. S. Hor, R. J. Cava, and M. Z. Hasan, Nature **452**, 970 (2008).
- <sup>13</sup> D. Hsieh, Y. Xia, L. Wray, D. Qian, A. Pal, J. H. Dil, J. Osterwalder, F. Meier, G. Bihlmayer, C. L. Kane, Y. S. Hor, R. J. Cava, and M. Z. Hasan, Science **323**, 919 (2009).
- <sup>14</sup> D. Hsieh, Y. Xia, D. Qian, L. Wray, J. H. Dil, F. Meier, J. Osterwalder, L. Patthey, J. G. Checkelsky, N. P. Ong, A. V. Fedorov, H. Lin, A. Bansil, D. Grauer, Y. S. Hor, R. J. Cava, and M. Z. Hasan, Nature **460**, 1101 (2009).
- <sup>15</sup> D. Hsieh, Y. Xia, D. Qian, L. Wray, F. Meier, J. H. Dil, J. Osterwalder, L. Patthey, A. V. Fedorov, H. Lin, A. Bansil, D. Grauer, Y. S. Hor, R. J. Cava, and M. Z. Hasan, Phys. Rev. Lett. **103**, 146401 (2009).
- <sup>16</sup> Y. Xia, D. Qian, D. Hsieh, L. Wray, A. Pal, H. Lin, A. Bansil, D. Grauer, Y. S. Hor, R. J. Cava, and M. Z. Hasan, Nat. Phys. **5**, 398 (2009).
- <sup>17</sup> Y. L. Chen, J. G. Analytis, J.-H. Chu, Z. K. Liu, S.-K. Mo, X. L. Qi, H. J. Zhang, D. H. Lu, X. Dai, Z. Fang, S. C. Zhang, I. R. Fisher, Z. Hussain, and Z.-X. Shen, Science **325**, 178 (2009).
- <sup>18</sup> A. Nishide, A. A. Taskin, Y. Takeichi, T. Okuda, A. Kakizaki, T. Hirahara, K. Nakatsuji, F. Komori, Y. Ando, and I. Matsuda, Phys. Rev. B **81**, 041309(R) (2010).
- <sup>19</sup> P. Roushan, J. Seo, C. V. Parker, Y. S. Hor, D. Hsieh, D. Qian, A. Richardella, M. Z. Hasan, R. J. Cava, and A. Yazdani, Nature **460**, 1106 (2009).
- <sup>20</sup> T. Zhang, Peng Cheng, X. Chen, J.-F. Jia, X. Ma, K. He, L. Wang, H. Zhang, X. Dai, Z. Fang, X. Xie, and Q.-K. Xue, Phys. Rev. Lett. **103**, 266803 (2009).
- <sup>21</sup> A. A. Taskin and Y. Ando, Phys. Rev. B **80**, 085303 (2009).
- <sup>22</sup> J. G. Checkelsky, Y. S. Hor, M.-H. Liu, D.-X. Qu, R. J. Cava, and N. P. Ong, Phys. Rev. Lett. **103**, 246601 (2009).
- <sup>23</sup> H. Peng, K. Lai, D. Kong, S. Meister, Y. Chen, X.-L. Qi, S.-C. Zhang, Z.-X. Shen, and Y. Cui, Nature Materials, doi:10.1038/nmat2609.
- <sup>24</sup> R. Shindou and S. Murakami, Phys. Rev. B **79**, 045321 (2009).
- <sup>25</sup> A. P. Schnyder, S. Ryu, A. Furusaki, and A. W. W. Ludwig, Phys. Rev. B **78**, 195125 (2008).
- <sup>26</sup> Y. Ran, Y. Zhang, and A. Vishwanath, Nat. Phys. **5**, 298 (2009).
- <sup>27</sup> D.-H. Lee, Phys. Rev. Lett. **103**, 196804 (2009).
- <sup>28</sup> J. G. Analytis, J.-H. Chu, Y. Chen, F. Corredor, R. D. McDonald, Z. X. Shen, and I. R. Fisher, arXiv:1001.4050.
- <sup>29</sup> A. A. Taskin, K. Segawa, and Y. Ando, arXiv:1001.1607.
- <sup>30</sup> H. Köhler and A. Fabricius, Phys. Status Solidi (b) **71**, 487 (1975).
- <sup>31</sup> Strictly speaking, there is a subtle shoulder structure near 80 T in the Fourier transform shown in the inset of Fig. 3(a), which suggests that there may be a weak contribution from a second frequency. In fact, it is known<sup>32</sup> for  $\text{Bi}_2\text{Se}_3$  that the second conduction-band minima begin to be populated when  $n_e$  becomes high, and in our sample  $n_e$  is actually close to this onset. Nevertheless, the possible contribution of this second electron pocket in our sample is so weak that it has no consequence in the transport properties being analyzed.
- <sup>32</sup> H. Köhler and H. Fisher, Phys. Status Solidi (b) **69**, 349 (1975).
- <sup>33</sup> D. Shoenberg, *Magnetic Oscillations in Metals* (Cambridge University Press, 1984).
- <sup>34</sup> S. Das Sarma and F. Stern, Phys. Rev. B **32**, 8442 (1985).
- <sup>35</sup> B. K. Cooper and V. M. Yakovenko, Phys. Rev. Lett. **96**, 037001 (2006).
- <sup>36</sup> R. N. Zitter, Phys. Rev. **127**, 1471 (1962).
- <sup>37</sup> If we take  $C_1$ ,  $C_2$ , and  $C_3$  as the principal axes and write  $\mathbf{H} = (H_1, H_2, H_3)$ , the resistivity component  $\rho_{11}$  in a magnetic field of arbitrary direction may be expanded to the lowest order in  $H_i$  as  $\rho_{11} = \rho_{11}(0) + \rho_{11,11}H_1^2 + \rho_{11,22}H_2^2 + \rho_{11,33}H_3^2 + 2\rho_{11,23}H_2H_3$  (see Ref. 36). The cross term  $\rho_{11,23}$  is probably the source of the offset of the center of symmetry seen in the insets of Fig. 5.